PHYSICAL REVIEW LETTERS

Optimal Control of Effective Hamiltonians

Albert Verdeny,[1,2] Łukasz Rudnicki,[1,3] Cord A. Müller,[4,5] and Florian Mintert[1,2]

[1]*Freiburg Institute for Advanced Studies, Albert-Ludwigs-Universität, Albertstrasse 19, 79104 Freiburg, Germany*
[2]*Department of Physics, Imperial College London, London SW7 2AZ, United Kingdom*
[3]*Center for Theoretical Physics, Polish Academy of Sciences, Aleja Lotników 32/46, 02-668 Warsaw, Poland*
[4]*Centre for Quantum Technologies, National University of Singapore, Singapore 117543, Singapore*
[5]*Department of Physics, University of Konstanz, 78457 Konstanz, Germany*

We present a systematic scheme for the optimization of quantum simulations. Specifically, we show how polychromatic driving can be used to significantly improve the driving of Raman transitions in the Lambda system, which opens new possibilities for controlled driving-induced effective dynamics.

In the past few years, one of the most active and promising research fields has been the design of quantum simulators, i.e., engineered controllable quantum systems utilized to mimic the dynamics of other systems. With this, new insight is expected to be gained in a variety of phenomena like high-temperature fractional quantum Hall states [1], (non-)Abelian gauge fields [2,3], and even relativistic effects [4,5].

Driven systems provide a powerful tool to simulate desired effective dynamics. An important example is laser-assisted Raman transitions between different electronic states and/or localized states of trapped atoms, which is a central pillar in a large number of quantum simulations. Because the direct coupling between low-lying energy states via dipole transitions is often forbidden by selection rules, an intermediate auxiliary state with higher energy is usually used to mediate the coupling. This so-called Lambda system is then specifically configured to imprint phases required to realize various spin-orbit couplings [6,7] or to simulate the effect of gauge fields [8,9]. Other prominent examples of driving-induced effective dynamics include shaken lattices [10–12], lattices with modulated interactions [13], or driven graphene [14].

Even though driven systems provide a powerful approach to perform quantum simulations, they often rely on approximations that currently situate them still far from the ideal quantum simulator. For instance, in Raman transitions via a three-level Lambda system, the driving pulse produces an undesired population of the excited state. These deviations between the desired and simulated dynamics accumulate during the evolution and become considerable after a sufficiently long time. From the experimental side, however, spectacular progress has been made in the manipulation and control of quantum systems [15,16], so that accurate theoretical tools to choose the proper driving are necessary. The field of optimal control theory [17,18] aims at such precise manipulation but, so far, it has primarily targeted properties at single instances in

time [19–22] whereas we are rather concerned with the behavior of a system during a continuous time window.

In this Letter, we provide a general systematic approach to improve quantum simulations by using pulse shaping techniques of optimal control theory. We discuss in detail the optimal control of the Lambda system and rigorously show how an appropriately chosen polychromatic driving can significantly improve Raman transitions. As a result, we do not only provide a proof of principle for the optimal control of effective Hamiltonians but also optimize a building block used in a large variety of quantum simulations.

Consider the target dynamics $U_{\text{tg}} = e^{-iH_{\text{tg}}t}$ generated by the target Hamiltonian H_{tg} that we wish to simulate using a time-periodic driving Hamiltonian $H(t) = H(t + T)$. Its time-evolution operator $U(t) = \mathcal{T} \exp[-i \int_0^t H(t')dt']$ then admits the Floquet decomposition [23]

$$U(t) = \tilde{U}(t)U_{\text{eff}}(t). \qquad (1)$$

Here $\tilde{U}(t)$ is a T-periodic unitary satisfying $\tilde{U}(0) = \mathbb{1}$, $U_{\text{eff}}(t) = e^{-iH_{\text{eff}}t}$, and H_{eff} is a time-independent effective Hamiltonian defined via $U(T) = e^{-iH_{\text{eff}}T}$. $\tilde{U}$ describes fluctuations around the envelope evolution U_{eff}. These fluctuations become negligible if the dominant energy scale Ω_d of $H(t)$ is sufficiently small compared to the driving frequency $\omega = 2\pi/T$. In this case the low-energy or long-time dynamics of the periodically driven system is well described by H_{eff}, which in turn should be chosen to match the target Hamiltonian H_{tg} to be simulated. Suppose now that the driving $H(t)$ contains a set $\{f_n\}$ of control parameters. Our aim is to tune these parameters such that the dynamics U resembles the target dynamics U_{tg} as well as possible. Different choices of $\{f_n\}$ can result in similar effective dynamics, but produce different fluctuations. In order to ensure the optimal simulation of a given target Hamiltonian H_{tg} with the least fluctuations, our scheme therefore consists of the following. (i) Identifying the dependence of the effective Hamiltonian H_{eff} on the control

parameters $\{f_n\}$. Typically this can only be achieved in an approximate manner, where $H_{\text{eff}} = \sum_{k=0}^{r} H_{\text{eff}}^{(k)} + O(\Omega_d \epsilon^{r+1})$ is known up to order r of the small parameter $\epsilon = \Omega_d / \omega \ll 1$. (ii) Constraining $\{f_n\}$ so that $H_{\text{tg}} = H_{\text{eff}}$ to the same order r. (iii) Minimizing the target functional

$$\mathcal{F} = \frac{1}{T} \int_0^T \|U(t) - U_{\text{tg}}(t)\|^2 dt, \tag{2}$$

where $\| \cdot \|^2 = \text{Tr}(\cdot^\dagger \cdot)$ is the Hilbert-Schmidt norm, under the constrained control parameters allowed by (ii). Since $\mathcal{F}$ shall also be approximated to the order r consistent with (i)–(ii) we can evaluate (2) using the substitution $U = \tilde{U} U_{\text{tg}}$. As a result $\|U - U_{\text{tg}}\|^2 = \text{Tr}[2\mathbb{1} - \tilde{U} - \tilde{U}^\dagger]$, so that $\mathcal{F}$ depends solely on the eigenvalues of $\tilde{U}$ [24].

In order to calculate H_{eff}, $U(t)$, and $\mathcal{F}$, we use the Magnus expansion [25,26] and write $U(t) = e^{-iM(t)}$ as the exponential of a time-dependent operator $M(t) = \sum_{k=1}^{\infty} M_k(t)$. The first two terms of this series are $M_1(t) = \int_0^t H(t_1) dt_1$ and

$$M_2(t) = -\frac{i}{2} \int_0^t dt_1 \int_0^{t_1} dt_2 [H(t_1), H(t_2)]. \tag{3}$$

The kth-order Magnus operator $M_k(t)$ contains k-fold time integrals of $k - 1$ nested commutators. When $H(t)$ is T periodic, $M_k(t)$ is exactly of order ϵ^k. Thus, $H_{\text{eff}}^{(k)} = M_{k+1}(T)/T \sim \Omega_d \epsilon^k$, since the factor $1/T = \omega/2\pi$ reduces the order of expansion by one. In this manner, H_{eff}, $U(t)$, and consequently $\mathcal{F}$ are determined up to order r, and our scheme (i)–(iii) yields parameters $\{f_n\}$ that ensure the optimal simulation of H_{tg}.

In the following, we exemplify the method described above with a case study of the degenerate Lambda system where $|1\rangle$ and $|2\rangle$ denote the two ground states and $|3\rangle$ the excited state. The target Hamiltonian

$$H_{\text{tg}} = -\Omega_{\text{tg}}(|1\rangle\langle 2| + |2\rangle\langle 1|) \tag{4}$$

generates Raman transitions within the ground-state manifold at a rate Ω_{tg} (the overall sign is chosen for later convenience). Our aim is to simulate this dynamics by driving the transitions $|1\rangle \leftrightarrow |3\rangle$ and $|2\rangle \leftrightarrow |3\rangle$ with a suitably modulated Rabi frequency. In the interaction picture, where the dynamics induced by the static Hamiltonian is absorbed in the state vectors, the driving Hamiltonian takes the form

$$H(t) = f(t)(1 + e^{-in_0 \Delta t})(|1\rangle\langle 3| + |2\rangle\langle 3|) + \text{H.c.} \tag{5}$$

Importantly, we assume that the driving pulse

$$f(t) = \sum_{n=1}^{N} f_n e^{-in\omega t} \tag{6}$$

is written as a general Fourier series in terms of ω, the fundamental frequency of driving. Since we do not want the

optimization to rely on strong intensity and fast frequencies, the maximal frequency in the above pulse is the detuning $\Delta = N\omega$, i.e., the difference of the resonance frequency of the Lambda system and the frequency of the driving carrier. That means that no Fourier components with frequency larger than Δ need to be generated. $H(t)$ defined in Eq. (5) should be periodic with period $T = 2\pi/\omega$, which is the case if Δ is a fraction of twice the driving carrier frequency, such that n_0 is a integer. In the rotating wave approximation, one would neglect the counterrotating contribution $e^{-in_0\Delta t}$ in Eq. (5); we consider the general case and keep this term.

Let us first discuss the simplest example of a monochromatic (MC) driving $f(t) = f_1 e^{-i\Delta t}$ at constant Rabi frequency by taking $N = 1$ in Eq. (6). Since the Magnus operator $M_{2l}(t)$ of the even order contains even products of $H(t)$, the corresponding effective Hamiltonian $H_{\text{eff}}^{(2l-1)}$ has the desired structure of H_{tg} with matrix elements that couple the ground states [27]. Choosing

$$|f_1|^2 = \Omega_{\text{tg}} \Delta \frac{1 + n_0}{2 + n_0}, \tag{7}$$

the constraint $H_{\text{eff}}^{(1)} = H_{\text{tg}}$ can be fulfilled to first order since $H_{\text{eff}}^{(0)} = 0$. The second-order term $H_{\text{eff}}^{(2)}$, on the other hand, will generate undesired transitions to the upper level via cubic powers of $H(t)$. With f_1 already fixed, one cannot impose $H_{\text{eff}}^{(2)} = 0$, so that one always ends up with an unwanted population in the excited state—except in the ideal limit of very strong, far-detuned driving $|f_1|, \Delta \to \infty$ at fixed Ω_{tg}. Thus, with only one frequency, one can neither accurately realize the desired unitary ground-state dynamics nor simultaneously minimize the fluctuations.

Let us then take advantage of the general pulse, Eq. (6), and implement the first constraint $H_{\text{eff}}^{(1)} = H_{\text{tg}}$ with

$$\Omega_{\text{tg}} = \frac{1}{\omega} \sum_{n=1}^{N} \frac{|f_n|^2}{\tilde{n}(1)}, \tag{8}$$

where $\tilde{n}(p)^{-1} \equiv n^{-p} + (n + Nn_0)^{-p}$. [In the rotating wave approximation $n_0 \to \infty$ this simplifies to $\tilde{n}(p) = n^p$.] Pushing the Magnus expansion to third order, we can now require $H_{\text{eff}}^{(2)} = 0$ through the second constraint

$$0 = \sum_{n=1}^{N} \frac{f_n}{\tilde{n}(1)}. \tag{9}$$

The target functional to be minimized reads [24]

$$\mathcal{F}^{(2)} = \frac{4}{\omega^2} \sum_{n=1}^{N} \frac{|f_n|^2}{\tilde{n}(2)}. \tag{10}$$

We can solve the optimization problem now analytically by introducing two Lagrange multipliers $\lambda_1 \in \mathbb{R}$, $\lambda_2 \in \mathbb{C}$ for

the two constraints, Eqs. (8) and (9), respectively. The optimal pulse parameters are found to be

$$f_n = \omega \lambda_2 \left(\frac{\tilde{n}(1)}{\tilde{n}(2)} - \lambda_1 \right)^{-1}. \qquad (11)$$

The Lagrange multipliers are determined by inserting this solution into the constraints, Eqs. (8) and (9). Dividing Eq. (11) by λ_2 shows that f_n/λ_2 is real, and thus all f_n as well as λ_2 can be taken as real. Using Eqs. (8) and (9), the target functional equation (10) can be rewritten as [24] $\mathcal{F}^{(2)} = 4\lambda_1 \Omega_{\text{tg}}/\omega$, such that the global minimum of the fluctuations is found with the minimal root λ_1 of Eq. (9) with Eq. (11) inserted. At a given value of ω, one should be able to suppress fluctuations more efficiently using more frequencies, and indeed, as $N \to \infty$ the minimal λ_1 tends to $\tilde{N}(1)/\tilde{N}(2) \sim 1/N$, such that $\mathcal{F}^{(2)} \to 0$.

With relatively little effort, one can take the calculation one step further. Using the first four terms of the Magnus expansion, the constraint equation (8) can be extended to third order $H_{\text{eff}}^{(1)} + H_{\text{eff}}^{(3)} = H_{\text{tg}}$ with the constraint

$$\Omega_{\text{tg}} = \omega(A_1 + 2B_3 - 4A_1A_2) \qquad (12)$$

defined in terms of $A_p = \sum |f_n/\omega|^2/\tilde{n}(p)$ and $B_p = \sum |f_n/\omega|^4/\tilde{n}(p)$. Equation (10) does not change to this order since $\mathcal{F}^{(3)} = 0$. The optimal Fourier components $\{f_n\}$ can still be chosen as real and solve the coupled system of equations ($n = 1, \dots, N$)

$$\frac{f_n}{\omega} \left[\frac{1 + 4A_1\lambda_1}{\tilde{n}(2)} - \lambda_1 \frac{1 - 4A_2}{\tilde{n}(1)} \right] - \frac{4\lambda_1 f_n^3}{\tilde{n}(3)\omega^3} = \frac{\lambda_2}{\tilde{n}(1)}. \qquad (13)$$

The full minimization in the third order of expansion, given by the system of Eqs. (13), (9) and (12), can be straightforwardly solved using the exact second-order solution equation (11) as an initial condition for a numerical routine.

A neat feature of the optimal pulse is that its total average intensity $I_N = \sum_{n=1}^{N} |f_n|^2$ never exceeds the intensity I_1 of the MC pulse. Since $\tilde{n}(p)^{-1}$ decreases with n, the right-hand side of (8) is lower bounded by $I_N/\omega\tilde{N}(1)$. From Eq. (7) we, however, get $I_1 = \Omega_{\text{tg}}\omega\tilde{N}(1)$ so $I_N \leq I_1$ for the second-order optimized pulse. Numerical evidence for the third-order optimized pulse confirms the relation $I_N \leq I_1$ in a broad range of N.

The suppression of fluctuations and deviations from desired dynamics polychromatic (PC) driving can be see in Fig. 1, where populations are depicted over half a period π/Ω_{tg} for a pulse with $N = 10$ frequencies. First of all, panels (a) and (b) of Fig. 1 depict the population of a low-lying state for short and long times, respectively. While the MC evolution with the Rabi frequency, Eq. (7), deviates significantly from the target evolution after several periods, the optimal PC dynamics follows the target rather
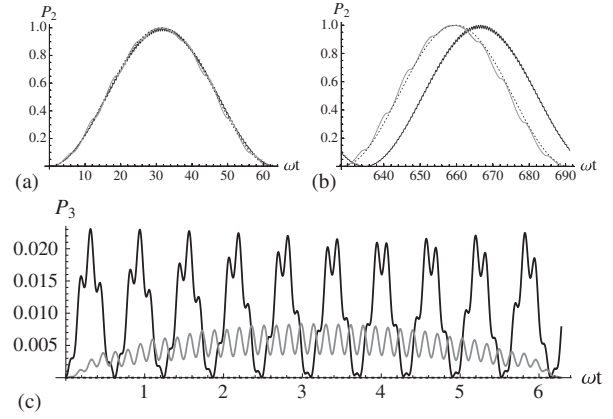

FIG. 1. (a) and (b) Transition probability $P_2(t) = |\langle 2|U(t)|1\rangle|^2$ for the target dynamics (dotted line), MC dynamics (black line), and third-order optimal dynamics with $N = 10$ frequency components (gray line). (c) Population of the excited state $P_3 = |\langle 3|U(t)|1\rangle|^2$ as a function of time. Plot parameters are $\Omega_{\text{tg}} = 0.05\omega$ and $n_0 = 4$.

faithfully. As the amplitude of the MC pulse has been chosen in first order, one might wonder if a better performance can be realized with an effective Hamiltonian that includes higher orders. Such a construction, however, would require a higher driving amplitude and, since the undesired terms in $H_{\text{eff}}^{(2)}$ cannot be set to zero, it results in larger overall deviations with respect to the target dynamics. Thus, an improvement of the MC case is not possible through a more accurate treatment. The lower panel (c) of Fig. 1 shows the second main advantage attributed to the short time scale of one driving period, namely, significantly smaller fluctuations of the optimal dynamics around the target dynamics and, in particular, a considerably lower population of the intermediate (excited) state.

In order to show to what extent the fluctuations can be suppressed, Fig. 2 depicts the deviations of the actual dynamics around the target unitary as a function of the number N of Fourier components. Both the analytic estimate (blue) and the numerically exact solution (red) show that already a moderate number of frequency components permits us to reduce the fluctuations dramatically. The Fourier components of the optimal pulse for $N = 10$ are shown in the inset. The component f_{10} of the highest frequency $\Delta = 10\omega$ is close to the MC solution (7); lower frequency components are phase shifted by π and their magnitude decays rapidly with decreasing frequency. These results show that modulating the driving with only few frequencies suffices to simulate the desired target unitary with significantly higher precision than in the MC case.

The long-time deviations observed in Fig. 1(b) can be quantitatively measured by the target functional $\mathcal{F}_n$, as defined in Eq. (2), but integrated over the nth driving period. In Fig. 3, these fidelities are shown for the MC pulse
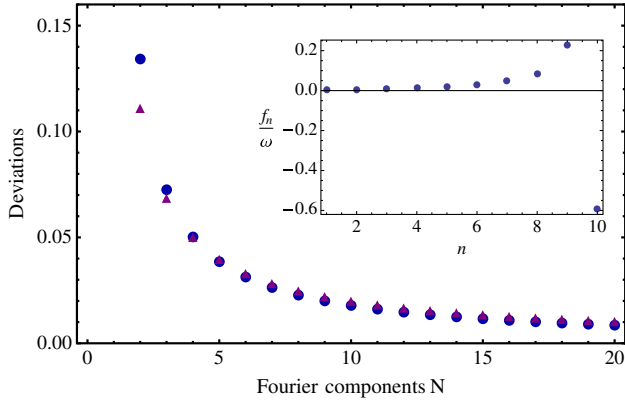
FIG. 2 (color online).   Magnitude of deviations around the target unitary dynamics as function of the number N of Fourier components. Blue dots depict the third-order target functional quantified by Eq. (10) and red triangles depict the numerically exact target functional, Eq. (2); plot parameters are $\Omega_{\text{tg}} = 0.05\omega$ and $n_0 = 4$. Inset: Fourier components for $N = 10$.

and the second- and third-order PC pulses with $N = 10$ as a function of n. Let us first compare the MC with the second-order PC pulse. In the first few periods, the optimized solution indeed yields a better result. However, the deviations with respect to the target dynamics grow faster in the second-order optimized case than in the MC case. As a consequence, in the long-time regime the MC driving performs better than the optimized solution calculated in second order: since the PC pulse contains slower frequencies than the MC one, the expansion at second order leads to a worse approximation of the effective Hamiltonian and the deviations between U_{eff} and U_{tg} accumulate in time and overcome the difference in fluctuations after sufficiently long times. Indeed, we observe that the larger
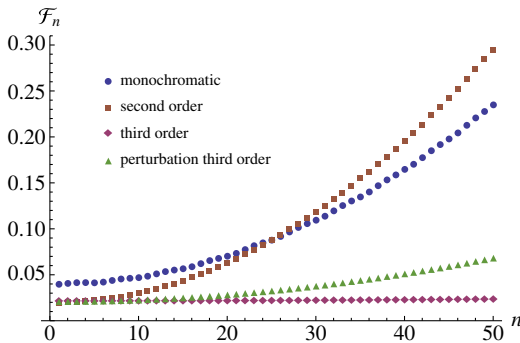

FIG. 3 (color online).   Deviations from the target dynamics $\mathcal{F}_n$ in the nth driving period [time interval $[(n-1)T, nT]$] for the MC pulse (blue circles), the second-order optimized pulse (brown squares), and the third-order optimized pulse (red rhombi) with $N = 10$. The perturbed third-order solution [see Eq. (14)] with frequency randomness $\delta = \delta_{\text{max}}/4$, averaged over 100 realizations (green triangles) shows good resilience against experimental uncertainty. $\Omega_{\text{tg}} = 0.05\omega$ and $n_0 = 4$.

N is, the later the crossover occurs, since the fluctuations are smaller and deviations from the target Hamiltonian need more time to accumulate to the value of the MC dynamics. Nevertheless, the optimized PC pulse can always be systematically improved by pushing the calculations to higher order in the expansion parameter. As seen in Fig. 1 as well as Fig. 3, the third-order optimal pulse significantly outperforms the MC dynamics in the entire time domain.

Finally, in order to estimate the robustness of optimal pulses in realistic experimental setups, we investigate how small perturbations to the Fourier components affect the performance of the optimal pulses. Consider perturbations of the form

$$f_n \to \tilde{f}_n = f_n + \delta f, \tag{14}$$

where δf is a random number uniformly distributed in the interval $[-\delta, \delta]$, which accounts for the experimental uncertainty in the tuned Fourier components. Comparison between the second- and third-order optimal pulses shows that their largest optimal Fourier components differ typically by 0.01ω (for $\Omega_{\text{tg}} = 0.05\omega$), which defines a scale δ_{max} for the maximum allowed uncertainty. Perturbations with $\delta = \delta_{\text{max}}/4$, however, still lead to a good performance; see Fig. 3. Thus, the optimal pulses appear robust under such perturbations, which indicates a good experimental viability. Moreover, the perturbed, optimized PC pulse provides a significantly lower level of deviations in comparison with the unperturbed MC pulse even after several periods $2\pi/\Omega_{\text{tg}}$.

The control of periodically driven systems by means of pulse shaping presented here opens new perspectives for the optimal simulation of quantum systems. No increase in intensity as compared to monochromatic driving is required and the realization of optimal effective Hamiltonians is robust under perturbations. Let us point out that the scalings of all parameters are algebraic, so that there is no exponential cost hidden in time, power, or number of Fourier components. The optimal pulses have a rather narrow spectral range, which eases the identification of driving parameters ensuring that no high lying states are excited. This is of particular importance for large many-body systems, like trapped atomic gases, where uncareful driving easily results in uncontrolled heating. Since this can be avoided with the present approach, it may, for example, be used to enhance or suppress long-range or density-dependent tunneling processes [28] in shaken optical lattices.

[1] E. Tang, J.-W. Mei, and X.-G. Wen, Phys. Rev. Lett. **106**, 236802 (2011).

[2] P. Hauke, O. Tieleman, A. Celi, C. Ölschläger, J. Simonet, J. Struck, M. Weinberg, P. Windpassinger, K. Sengstock, M. Lewenstein, and A. Eckardt, Phys. Rev. Lett. **109**, 145301 (2012).

[3] D. Banerjee, M. Bögli, M. Dalmonte, E. Rico, P. Stebler, U.-J. Wiese, and P. Zoller, Phys. Rev. Lett. **110**, 125303 (2013).

[4] N. Goldman, A. Kubasiak, A. Bermudez, P. Gaspard, M. Lewenstein, and M. A. Martin-Delgado, Phys. Rev. Lett. **103**, 035301 (2009).

[5] J. A. Franco-Villafañe, E. Sadurní, S. Barkhofen, U. Kuhl, F. Mortessagne, and T. H. Seligman, Phys. Rev. Lett. **111**, 170405 (2013).

[6] L. W. Cheuk, A. T. Sommer, Z. Hadzibabic, T. Yefsah, W. S. Bakr, and M. W. Zwierlein, Phys. Rev. Lett. **109**, 095302 (2012).

[7] P. Wang, Z.-Q. Yu, Z. Fu, J. Miao, L. Huang, S. Chai, H. Zhai, and J. Zhang, Phys. Rev. Lett. **109**, 095301 (2012).

[8] H. Miyake, G. A. Siviloglou, C. J. Kennedy, W. C. Burton, and W. Ketterle, Phys. Rev. Lett. **111**, 185302 (2013).

[9] M. Aidelsburger, M. Atala, M. Lohse, J. T. Barreiro, B. Paredes, and I. Bloch, Phys. Rev. Lett. **111**, 185301 (2013).

[10] A. Eckardt, C. Weiss, and M. Holthaus, Phys. Rev. Lett. **95**, 260404 (2005).

[11] H. Lignier, C. Sias, D. Ciampini, Y. Singh, A. Zenesini, O. Morsch, and E. Arimondo, Phys. Rev. Lett. **99**, 220403 (2007).

[12] J. Struck, C. Ölschläger, M. Weinberg, P. Hauke, J. Simonet, A. Eckardt, M. Lewenstein, K. Sengstock, and P. Windpassinger, Phys. Rev. Lett. **108**, 225304 (2012).

[13] A. Rapp, X. Deng, and L. Santos, Phys. Rev. Lett. **109**, 203005 (2012).

[14] T. Iadecola, D. Campbell, C. Chamon, C.-Y. Hou, R. Jackiw, S.-Y. Pi, and S. V. Kusminskiy, Phys. Rev. Lett. **110**, 176603 (2013).

[15] S. Braun, J. P. Ronzheimer, M. Schreiber, S. S. Hodgman, T. Rom, I. Bloch, and U. Schneider, Science **339**, 52 (2013).

[16] J. Struck, M. Weinberg, C. Olschlager, P. Windpassinger, J. Simonet, K. Sengstock, R. Hoppner, P. Hauke, A. Eckardt, M. Lewenstein, and L. Mathey, Nat. Phys. **9**, 738 (2013).

[17] D. D'Alessandro, *Introduction to Quantum Control and Dynamics* (CRC, Boca Raton, 2007).

[18] V. F. Krotov, *Global Methods in Optimal Control Theory* (Marcel Dekker, New York, 1996).

[19] N. Khaneja, T. Reiss, C. Kehlet, T. Schulte-Herbrüggen, and S. J. Glaser, J. Magn. Reson. **172**, 296 (2005).

[20] B. Rogers, M. Paternostro, G. M. Palma, and G. De Chiara, Phys. Rev. A **86**, 042323 (2012).

[21] D. M. Reich, G. Gualdi, and C. P. Koch, Phys. Rev. Lett. **111**, 200401 (2013).

[22] B. Bartels and F. Mintert, Phys. Rev. A **88**, 052315 (2013).

[23] G. Floquet, Ann. École Norm. Sup. **12**, 47 (1883).

[24] See the Supplemental Material at http://link.aps.org/supplemental/10.1103/PhysRevLett.113.010501 for the technical aspects.

[25] W. Magnus, Commun. Pure Appl. Math. **7**, 649 (1954).

[26] S. Blanes, F. Casas, J. Oteo, and J. Ros, Phys. Rep. **470**, 151 (2009).

[27] These terms also generate light-shift displacements of the excited and ground states which do not influence the target dynamics between the two ground states.

[28] A. Verdeny, A. Mielke, and F. Mintert, Phys. Rev. Lett. **111**, 175301 (2013).

Supplemental Material for *Optimal Control of Effective Hamiltonians*

Albert Verdeny,[1,2] Łukasz Rudnicki,[1,3] Cord A. Müller,[4,5] and Florian Mintert[1,2]

[1]*Freiburg Institute for Advanced Studies, Albert-Ludwigs-Universität, Albertstrasse 19, 79104 Freiburg, Germany*
[2]*Department of Physics, Imperial College London, London SW7 2AZ, United Kingdom*
[3]*Center for Theoretical Physics, Polish Academy of Sciences, Aleja Lotników 32/46, 02-668 Warsaw, Poland*
[4]*Centre for Quantum Technologies, National University of Singapore, Singapore 117543, Singapore*
[5]*Department of Physics, University of Konstanz, 78457 Konstanz, Germany*
(Dated: May 9, 2014)

In this Supplemental Material, several technical aspects of the analytic minimization are given in detail in order to ease the reproduction of our results. According to our scheme (i-iii) in the main paper, the target functional (TF) Eq. (2) and the constraints Eq. (8), Eq. (9) are the starting point for the minimization . While the constraints are straightforwardly derived using the Magnus expansion, the expressions for the TF require a more detailed explanation.

This Supplemental Material is divided into three sections:

- In Sec. I, some general aspects regarding the calculation of the target functional are explained.

- In Sec. II, the derivation of the TF of the Lambda system expanded up to third order

$$\sum_{k=0}^{3} \mathcal{F}^{(k)} = \frac{4}{\omega^2} \sum_{n=1}^{N} \frac{|f_n|^2}{\tilde{n}(2)} \qquad (s1)$$

is given in detail.

- In Sec. III, the expression

$$\mathcal{F}^{(2)} = 4\lambda_1 \frac{\Omega_{\text{tg}}}{\omega} \qquad (s2)$$

that yields the second order global minimum is derived.

I. GENERAL TARGET FUNCTIONAL

Given the decomposition $U(t) = \tilde{U}(t)U_{\text{eff}}(t)$, the TF defined in Eq. (2) can be written as

$$\mathcal{F} = \frac{1}{T} \int_0^T \text{Tr}\left[2\mathbb{1} - \tilde{U}U_{\text{eff}}U_{\text{tg}}^\dagger - U_{\text{tg}}U_{\text{eff}}^\dagger \tilde{U}^\dagger \right] dt. \quad (s3)$$

Under the constraint $H_{\text{tg}} = H_{\text{eff}}$, the TF simplifies to

$$\mathcal{F} = \frac{1}{T} \int_0^T \text{Tr}\left[2\mathbb{1} - \tilde{U} - \tilde{U}^\dagger \right] dt$$

$$= \frac{2}{T} \int_0^T \left(d - \sum_i^d \cos(\nu_i(t)) \right) dt, \qquad (s4)$$

where d is the dimension of the Hilbert space and $\nu_i(t)$ are the eigenvalues of $G(t)$ defined via $\tilde{U}(t) = e^{-iG(t)}$.

If the constraint is only satisfied up to a certain order r, $H_{\text{tg}} = \sum_{k=0}^{r} H_{\text{eff}}^{(k)} + O(\Omega_d \epsilon^{r+1})$, Eq. (s4) is to be taken up to the same order, $\mathcal{F} = \sum_{k=0}^{r} \mathcal{F}^{(k)} + O(\epsilon^{r+1})$. Similarly as with the effective Hamiltonian, an expansion $G(t) = \sum_{k=1}^{r} G^{(k)}(t) + O(\epsilon^{r+1})$ can be obtained with the Magnus expansion and the Baker-Cambell-Hausdorff formula. The first two terms read:

$$G^{(1)}(t) = M_1(t) - H_{\text{eff}}^{(0)} t, \qquad (s5)$$

$$G^{(2)}(t) = M_2(t) - H_{\text{eff}}^{(1)} t + \frac{i}{2}[G^{(1)}(t), H_{\text{eff}}^{(0)} t]. \quad (s6)$$

II. TARGET FUNCTIONAL FOR THE LAMBDA SYSTEM

For the Lambda system described by Eq. (5), the first two leading terms of $G(t)$ are

$$G^{(1)}(t) = g_1(|1\rangle\langle 3| + |2\rangle\langle 3|) + H.c., \qquad (s7)$$

$$G^{(2)}(t) = g_2\left((|1\rangle + |2\rangle)(\langle 1| + \langle 2|) - 2|3\rangle\langle 3|\right), \quad (s8)$$

where

$$g_1 = i\sum_n \frac{f_n}{\omega n}(e^{-in\omega t} - 1)$$

$$+ i\sum_n \frac{f_n}{\omega(n + Nn_0)}(e^{-i(n+Nn_0)\omega t} - 1). \quad (s9)$$

The second order term g_2 will not contribute to the final result. The eigenvalues of the sum $G^{(1)}(t) + G^{(2)}(t)$ are $\{\nu_1, \nu_2, \nu_3\} = \{0, \pm\sqrt{2(|g_1|^2 + 2g_2^2)}\}$. Consistently with our expansion in ϵ, the cosine in Eq. (s4) can be expanded in a Taylor series up to second order in its argument, namely $(d = 3)$

$$\sum_{k=0}^{3} \mathcal{F}^{(k)} = \frac{2}{T} \int_0^T \left(3 - \sum_{i=1}^{3} \left(1 - \frac{\nu_i^2(t)}{2}\right)\right) dt$$

$$= \frac{2}{T} \int_0^T \sum_{i=1}^{3} \frac{\nu_i^2(t)}{2} dt. \qquad (s10)$$

As the eigenvalues $\nu_i(t)$ enter quadratically in (s10), the only contribution to the TF is given by $G^{(1)}(t)$; $G^{(2)}(t)$ and higher orders of the cosine yield contributions of fourth or higher order in ϵ. Thus

$$\sum_{k=0}^{3} \mathcal{F}^{(k)} = \mathcal{F}^{(2)} = \frac{4}{T} \int_0^T |g_1|^2 dt. \qquad (s11)$$

Using the expression Eq. (s9) and the constraint (9) results in Eq. (s1).

III.   MINIMIZATION IN SECOND ORDER

A crucial point for the analytic results obtained in second order is the possibility to write the target functional in terms of the Lagrange multiplier λ_1 as in Eq. (s2), which permits us to obtain the global minimum of $\mathcal{F}^{(2)}$.

The TF to be minimized and the two constraints

$$C_1 = \sum_n \frac{|f_n|^2}{\omega^2 \tilde{n}(1)} - \frac{\Omega_{\text{tg}}}{\omega} \quad \text{and} \quad C_2 = \sum_n \frac{f_n^*}{\omega \tilde{n}(1)} \quad \text{(s12)}$$

define the Lagrange functional

$$\mathcal{L}[f_n, f_n^*, \lambda_1, \lambda_2] = \mathcal{F}^{(2)}/4 - \lambda_1 C_1 - \lambda_2 C_2. \quad \text{(s13)}$$

The extrema of $\mathcal{L}$ are given by the system of Eqs. (8), (9) and (11), which are found after differentiating (s13) with respect to λ_1, λ_2 and f_n^* respectively. After inserting Eq. (11) into Eqs. (8) and (9), two equations for the Lagrange multipliers are obtained

$$0 = \sum_{n=1}^{N} \left(\frac{\tilde{n}(1)^2}{\tilde{n}(2)} - \lambda_1 \tilde{n}(1) \right)^{-1}, \quad \text{(s14)}$$

$$|\lambda_2| = \sqrt{\frac{\Omega_{\text{tg}}}{\omega} \left(\sum_{n=1}^{N} \tilde{n}(1) \left(\frac{\tilde{n}(1)^2}{\tilde{n}(2)} - \lambda_1 \tilde{n}(1) \right)^{-2} \right)^{-1/2}} \quad \text{(s15)}$$

Eq. (s15) can be rewritten using (s14) as

$$|\lambda_2| = \sqrt{\frac{\Omega_{\text{tg}}}{\omega} \left(\sum_{n=1}^{N} \left(\tilde{n}(1) - \frac{\tilde{n}(1)^2}{\lambda_1 \tilde{n}(2)} + \frac{\tilde{n}(1)^2}{\lambda_1 \tilde{n}(2)} \right) \left(\frac{\tilde{n}(1)^2}{\tilde{n}(2)} - \lambda_1 \tilde{n}(1) \right)^{-2} \right)^{-1/2}}$$

$$= \sqrt{\frac{\lambda_1 \Omega_{\text{tg}}}{\omega} \left(\sum_{n=1}^{N} \frac{\tilde{n}(1)^2}{\tilde{n}(2)} \left(\frac{\tilde{n}(1)^2}{\tilde{n}(2)} - \lambda_1 \tilde{n}(1) \right)^{-2} \right)^{-1/2}}. \quad \text{(s16)}$$

Finally, inserting Eq. (11) into Eq. (10) and using Eq. (s16) above results in Eq. (s2).